Perovskite Solar Cells

Deutsche Ausgabe: DOI: 10.1002/ange.201606574
Internationale Ausgabe: DOI: 10.1002/anie.201606574

Limiting Perovskite Solar Cell Performance by Heterogeneous Carrier Extraction

Wenming Tian, Rongrong Cui, Jing Leng, Junxue Liu, Yajuan Li, Chunyi Zhao, Jun Zhang, Weiqiao Deng, Tianquan Lian, and Shengye Jin**

Abstract: *Although the power conversion efficiency of perovskite solar cells has improved rapidly, a rational path for further improvement remains unclear. The effect of large morphological heterogeneity of polycrystalline perovskite films on their device performance by photoluminescence (PL) microscopy has now been studied. Contrary to the common belief on the deleterious effect of morphological heterogeneity on carrier lifetimes and diffusivities, in neat $CH_3NH_3PbI_3(Cl)$ polycrystalline perovskite films, the local (intra-grain) carrier diffusivities in different grains are all surprisingly high (1.5 to 3.3 cm^2s^{-1}; comparable to bulk single-crystals), and the local carrier lifetimes are long (ca. 200 ns) and surprisingly homogenous among grains, and uniform across grain boundary and interior. However, there is a large heterogeneity of carrier extraction efficiency at the perovskite grain–electrode interface. Improving homogeneity at perovskite grain–electrode contacts is thus a promising direction for improving the performance of perovskite thin-film solar cells.*

Organolead halide perovskite solar cells, with a certified power conversion efficiency of 22.1 %,[1] have received intense attention in recent years.[2–12] Although it has been recognized that carrier (electron and hole) diffusion lengths (a product of carrier diffusivity/mobility and lifetime) and extraction efficiency are key parameters affecting device performance,[13,14] a reliable determination and rational improvement of these key material properties has been hindered by large heterogeneities in the grain sizes, shapes, and grain boundaries of typical perovskite thin films fabricated by either solution processing or vapor deposition. Most charge mobility measurements, by techniques such as photoluminescence (PL) quenching,[11,15] transient spectroscopy,[13,14,16] time-of-flight,[17,18] and hall effect,[19] probe the average bulk values of diffusion parameters (carrier diffusivity and mobility), lacking the ability to differentiate intra- vs. inter-grain transport properties. The reported charge mobility values in perovskite polycrystalline films differ by orders of magnitude (10^{-5} to 10 $s\,cm^2\,V^{-1}\,s^{-1}$)[20–22] and are much smaller than the value of bulk single crystals (about 100 to 150 $cm^2\,V^{-1}\,s^{-1}$),[17,18,23] which has been partially attributed to the heterogeneous distribution of grain size, grain boundary, and defects.[24]

Recent imaging studies have reported that PL or cathodoluminescence intensity and decay kinetics varied greatly (<10 ns to 100 s ns) from grain to grain and from grain interior to boundaries even in large-grained and high performing perovskite thin films.[25–29] These spatial variations of PL decays are attributed to a heterogeneous distribution of defects, which induce fast non-radiative carrier recombination,[25,28,29] and grain boundaries are believed to be the major regions with higher defect densities.[25] In contrary, some other theoretical and experimental studies also suggested that grain boundaries have negligible or even beneficial impact on the performance of perovskite solar cells.[30,31] It has also been noted in confocal microscopy imaging measurements where the excitation laser is focused in a diffraction limited spot (typically <1 μm), the observed PL kinetics contains contribution of carrier diffusion out of the excitation/PL collection spot, which can influence the reliable determination of the spatial variation of intrinsic carrier lifetime.[23,32] Nevertheless, it is now widely believed that the morphological heterogeneity incurs deleterious local optoelectronic properties in perovskite films,[25–29,33] although the mechanism by which the morphology influence performance remains unclear. Thus, the ability to probe the effect of morphological heterogeneity on carrier lifetime and mobility and the consequent device performance is essential for the rational improvement of solar cell performance.[33,34]

Herein, we report a study of carrier lifetime, intra- and inter- grain carrier diffusion coefficients, carrier diffusion length, and carrier extraction efficiency with sub-micrometer (and sub-grain) spatial resolution. Accounting properly for fast carrier diffusion, both the carrier diffusivity and lifetime can be imaged by photoluminescence (PL) microscopy. We observed that the local (intra-grain) carrier diffusivities in high performing hybrid $CH_3NH_3PbI_3(Cl)$ perovskite polycrystalline films are remarkably high, similar to the values in bulk single crystals,[17,18,23] and carrier lifetimes are long and surprisingly uniform among grains of different sizes and shapes and across grain interior and boundary. In the

[*] Dr. W. Tian, R. Cui, Dr. J. Leng, Y. Li, C. Zhao, Prof. Dr. W. Deng, Prof. Dr. S. Jin
State Key Laboratory of Molecular Reaction Dynamics
Dalian Institute of Chemical Physics,
Chinese Academy of Sciences; Collaborative Innovation Center of Chemistry for Energy Materials (iChEM)
457 ZhongShan Rd., Dalian, 116023 (China)
E-mail: sjin@dicp.ac.cn
J. Liu, Prof. Dr. J. Zhang
Department of Chemistry, China University of Petroleum
66 Changjiang West Rd., Huangdao District
Qingdao, 266580 (China)
Prof. Dr. T. Lian
Department of Chemistry, Emory Univeristy
1515 Dickey Drive, Atlanta, GA (USA)
E-mail: tlian@emory.edu

Supporting information for this article can be found under: http://dx.doi.org/10.1002/anie.201606574.

 © 2016 Wiley-VCH Verlag GmbH & Co. KGaA, Weinheim

presence of electron- or hole-accepting layers, the efficiency of carrier extraction to these layers show large grain-to-grain heterogeneity, which is due to the presence of defects at the perovskite–electron (hole) acceptor interface. Because of the low lateral inter-grain diffusivities, the carriers in these grains cannot find alternative collecting pathways, which is likely a key factor limiting the further improvement of device performance.

Our PL imaging measurements for local carrier diffusivity and lifetime were carried out on $CH_3NH_3PbI_3(Cl)$ polycrystalline thin films prepared by spin-coating the mixed halide precursor solution ($CH_3NH_3I/PbCl_2 = 3:1$ in *N*,*N*-dimethylformamide) on a glass coverslip (see the Supporting Information for details).[25] The scanning electron microscopy (SEM) (Figure 1a) and optical (Figure 1b) images show

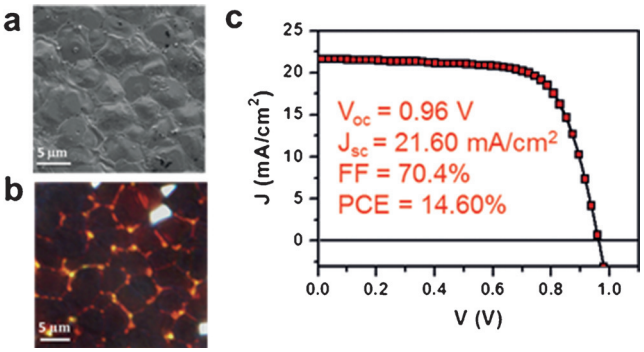

Figure 1. a) SEM and b) TEM optical images of a $CH_3NH_3PbI_3$ polycrystalline film grown on a glass coverslip. c) Photocurrent–voltage (*J*–*V*) characterization of a $CH_3NH_3PbI_3$ perovskite solar cell.

a typical grain size of about a few micrometers. Using the same perovskite film fabrication procedure (see the Supporting Information for details), we also constructed solar cells exhibiting power conversion efficiency of as high as 14.6% (Figure 1c; Supporting Information, Figure S1).

First, we directly measure the intra-grain (local) and inter-grain carrier diffusivity (D) in polycrystalline perovskite films by the PL-scanned imaging microscopy (see Figure S2 and optical measurements in the Supporting Information). Briefly, the grains were excited by a focused laser beam (680 nm, 1 MHz, 1.6 μJ cm^{-2} per pulse) with a radius of about 0.6 μm. By scanning the PL collection spot over the grains with a fixed excitation position, we constructed the PL intensity images (Figure 2a and c; Supporting Information, Figure S3). The PL kinetics extracted at a few micrometers away from the excitation spot (after subtracting the wave-guiding components; Supporting Information, Figure S4) shows a slow rise and decay (Figure 2b and d; Supporting Information, Figure S4), indicative of carrier transport and recombination processes. These kinetics can be fit by numerically solving a diffusion model (see the Supporting Information) that accounts for lateral carrier diffusion and local carrier decay. The fits yield the diffusivity *D* of the examined grains.

In Table 1, we listed the intra-grain carrier diffusivity for nine grains (grains 1 to 9; Supporting Information, Figure S3a) in a polycrystalline perovskite film. The diffusivity does not vary significantly from grain to grain (1.5 to 3.3 cm^2 s^{-1}), and these values are larger by one to two orders of magnitude than the local diffusivity reported for polycrystalline films using ultrafast transient absorption microscopy,[34] and are similar to those reported for $CH_3NH_3PbI_3$ single crystals.[17,18,23] We also observed that the carrier diffusion is largely confined within the grains, with negligible inter-grain diffusivity (Figure 2b). Only a few grains show carrier transport across the grain boundaries (Figure 2c), where the inter-grain diffusivity is reduced by almost 50% compared to intra-grain diffusivity. Carrier scattering at grain boundaries is likely the major factor that limits the inter-grain carrier transport, but the extent of this limitation likely depends on

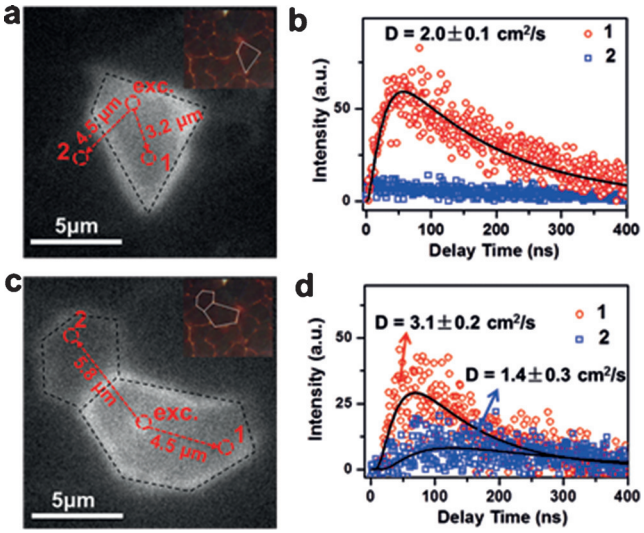

Figure 2. a) and c) PL intensity images of individual grains obtained by the PL-scanned imaging microscopy with the focused laser beam (680 nm, 1 MHz, 1.6 μJ cm^{-2}/pulse) fixed at the indicated positions (exc.). The dashed lines are the approximate boundary lines of the grains where the simulation of the carrier diffusion process is performed. Insets: optical images of the films showing the grains where the carrier diffusivity is measured. b) and d) PL kinetics extracted at spots 1 (for intra-grain diffusion) and 2 (for inter-grain diffusion) after subtracting the wave-guiding effects (see the Supporting Information, Figure S4). The solid lines are fits of the kinetics by a simulation program, from which the carrier diffusivity is determined.

Table 1: The measured carrier diffusivity (*D*), carrier lifetime (*τ*), and diffusion length (L_D) for the nine different selected perovskite grains with different sizes.[a]

Grain no.	Size [μm]	*D* [cm^2 s^{-1}]	*τ* [ns]	L_D [μm]
1	6.7	3.1	229	8.4
2	4.2	2.2	186	6.4
3	5.3	1.7	160	5.2
4	4.3	1.6	198	5.6
5	4.3	2.0	166	5.7
6	8.0	1.5	210	5.5
7	4.0	3.3	212	8.4
8	5.0	2.3	171	6.3
9	3.3	1.8	176	5.6

[a] Size estimated from the horizontal dimension.

© 2016 Wiley-VCH Verlag GmbH & Co. KGaA, Weinheim

how closely or tightly the neighboring grains are chemically or physically connected. The intra-grain carrier diffusivity revealed in this study are higher than most reported values (estimated by charge mobility) in perovskite polycrystalline films probed by ensemble averaged techniques.[11,13,14,16,19] Our result suggests that lower diffusivity reported in these previous measurements likely results from a slow inter-grain transport, which limits the overall diffusivity across the film.

Next, we measured the spatial distribution of intrinsic carrier lifetime using the PL-scanned imaging microscopic Scheme (Supporting Information, Figure S2). In conventional confocal PL microscopic measurements, the excitation laser beam is focused to a diffraction-limited spot (diameter < 1 μm) on the sample. Given the high local carrier diffusivity revealed in our measurement above, the confocal PL decay depends not only on the local carrier radiative and non-radiative decay processes, but also on lateral diffusion outside the small illumination/detection spot, as we will discuss below. The latter effect dominates the measured PL decay for perovskite materials with high carrier diffusivity and long intrinsic carrier lifetimes. Therefore, in our PL lifetime measurements, we used a uniform wide-field illumination (with diameter of about 60 μm, encompassing a few grains) on the sample while detecting emission from a diffraction-limited spot (Supporting Information, Figure S2). Because of slow inter-grain carrier diffusion, there is negligible effect of fast lateral carrier diffusion in a uniformly illuminated grain.

Figure 3a shows a wide-field-illuminated PL intensity image of a perovskite thin film on a glass coverslip recorded with 680 nm excitation (1 MHz and 96 nJ cm^{-2} per pulse). This image exhibits higher PL intensity along the grain boundaries, which can be attributed to the leak of wave-guided PL photons emitted by the film.[23] Surprisingly, we observed that the PL decays from all scanned spots show slow single-exponential kinetics. By fitting the PL decays with a single exponential function, we constructed a PL lifetime image of the perovskite film (Figure 3b), and representative decay kinetics and fits at selected positions (grain boundaries and interiors) are shown in Figure 3c. Statistical analysis of the lifetime image shows a remarkably homogeneous lifetime distribution (with an average of about 194 ns and a FWHM of 19 ns) across the entire circa 30×30 μm film area (Figure 3b), which is comparable to the ensemble average carrier lifetime in high performing solar cells.[8,11] This homogeneous distribution of PL lifetime persists even at increased excitation intensity (1.5 μJ cm^{-2}/pulse) when the fast-bimolecular carrier recombination component appears (Supporting Information, Figure S5). A simulation of the PL kinetics (Supporting Information, Figure S6) suggests that the lack of spatial dependence of the PL decay kinetics within the grains can be attributed to fast carrier diffusion, sampling the whole grain within their lifetime. In Table 1 and the Supporting Information, Figure S7, we compared the total PL decays (constructed by the photons from the entire grain) of nine selected grains, showing similar long PL decay lifetimes in all grains in spite of large variations in grain sizes, shapes and boundaries (Supporting Information, Figure S7b). This observation is further confirmed by the PL decay from a perovskite film with much smaller grain size (a few hundred nanometers) and higher density of grain boundary, which also shows a slow single exponential decay kinetics with a similar lifetime (Supporting Information, Figure S8). It is important to note that we have also verified that our PL imaging measurement is able to identify fast non-radiative quenching sites (with quenching rate $\geq 1 \times 10^8$ s^{-1}) if there are any in the perovskite grains (Supporting Information, Figure S9).

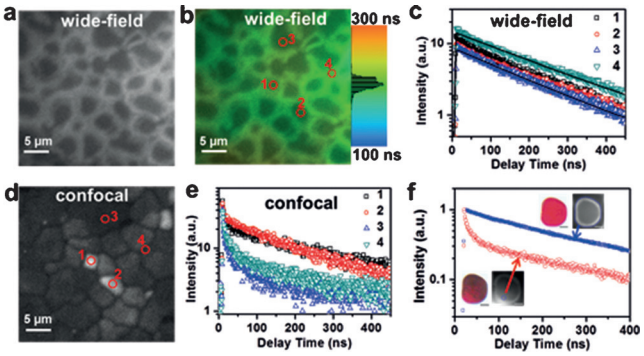

Figure 3. a) Wide-field-illuminated PL intensity and b) composite intensity (by brightness) and lifetime (by color) images of a perovskite thin film measured at 680 nm excitation (1 MHz repetition rate and 96 nJ cm^{-2} per pulse). The lifetime from each scanned spot is obtained by single exponential fit to PL decay. Also shown is a histogram of local carrier lifetimes in the studied area (30×30 μm^2). c) Comparison of local PL decay kinetics extracted at four selected positions (1–4) on the wide-field-illuminated PL image (symbols) and fits by a single exponential function (solid lines), showing similar decay kinetics. d) Confocal PL intensity image of the perovskite film on the same area as in (a) under the same excitation intensity and e) comparison of selected local PL decay kinetics, showing very different decay rates. f) Comparison of PL decays in an isolated $CH_3NH_3PbI_3$ perovskite grain with different excitation areas. Insets: optical and PL intensity images of the grain. Scale bars: 5 μm. The red color in the optical images indicates the coverage of excitation laser (wide-field illumination) on the grain. The grain shows a slow single-exponential decay (blue squares) when homogeneously excited; when partially excited, the PL decay extracted on a one micrometer spot (red circles) within the excitation area shows a fast component owing to fast lateral carrier diffusion.

The observed homogeneous distribution of local carrier lifetimes across the perovskite film in our wide-field-illuminated PL measurements contradicts the results of recent confocal PL studies.[25–29] To understand the origin of this discrepancy, we also collected the confocal PL image (with the same excitation intensity as in the wide-field illumination measurements) on the same area in the perovskite film (Figure 3d). We also observed grain-to-grain PL intensity (Figure 3d) and lifetime (Figure 3e) variations (with clearly faster kinetics in dark grains than in bright grains), even though these grains exhibit similar PL lifetime in the wide-field illumination measurement (Figure 3b). In the following, we demonstrated that the spatial variations in local PL intensity and kinetics shown in the confocal PL images are caused by fast intra-grain carrier diffusion away from the illuminated spot, instead of variations of local non-radiative decay rates. In Figure 3f, we compare the PL decay collected from a circa 1 μm spot (corresponding to the size of excitation/PL collection spot in the confocal measurement)

 © 2016 Wiley-VCH Verlag GmbH & Co. KGaA, Weinheim

in an isolated perovskite grain when an excitation area is smaller than the grain size and when the grain is uniformly illuminated (under wide-field illumination with 96 nJ cm^{-2} per pulse). We observed that under the former condition, the decay kinetics is biphasic with the slow component identical to the nearly single exponential decay observed under latter (uniform) illumination conditions. The fast component in the former kinetics, whose amplitude also depends on the spot size of excitation (Supporting Information, Figure S10), can be attributed to a rapid diffusion of carriers away from the excitation/PL collection spot, driven by the carrier density gradient. This interpretation is supported by a simulation that accounts for this lateral diffusion effect, which also shows that the amplitude of the diffusion-induced fast component can range from 0% to 90%, depending on the excitation/PL collection area and position relative to the size and shape of grains (Supporting Information, Figure S11). This diffusion-induced fast PL decay kinetics is particularly pronounced when the excitation and PL collection spot is smaller than the grain size, which is the case in most confocal microscopic measurements. The presence of fast carrier diffusion makes it difficult for confocal PL measurement to identify the quenching site within the grain (Supporting Information, Figure S12).

From the measured local carrier lifetime and diffusivity, the theoretical diffusion length (L_D) inside perovskite grains was calculated to range from 5 to 8 μm (Table 1). These values are comparable to or larger than the lateral size of the grains but much larger than their thickness. In perovskite thin film solar cells with grain sizes larger than the film thickness, this long carrier diffusion length ensures that carriers can be transported to the grain/collecting electrode interfaces by fast intra-grain diffusion. However if there exist defects at the perovskite grain/electrode interface, these carriers cannot find alternative collection pathways because of the slow lateral inter-grain diffusion. To investigate the effect of slow lateral inter-grain diffusion on carrier collection efficiencies, we mapped the PL quenching efficiency of the perovskite films after deposition of hole (Spiro-OMeTAD; Figure 4a) or electron (fullerene PCBM; Figure 4b) acceptor layers as in a solar cell device (see the Supporting Information for experimental details). The quenching efficiency (η) is calculated by the PL decay lifetimes from each position before and after the deposition of quenchers (Supporting Information, Figures S13 and S14). Notably, we observed that although the films show an effective η of about 80% in majority of grains, many grains show considerably smaller η down to 50–60% for Spiro-OMeTAD and 70% for PCBM. We attribute these poor PL quenching efficiencies to charge extraction defects at these grain–electron (hole) acceptor interfaces and the lack of alternatively carrier collection pathways caused by slow lateral inter-grain diffusion. We speculate that origin of this heterogeneity is likely caused by the inhomogeneity in interfacial contact structure between the perovskite and charge extraction layer.

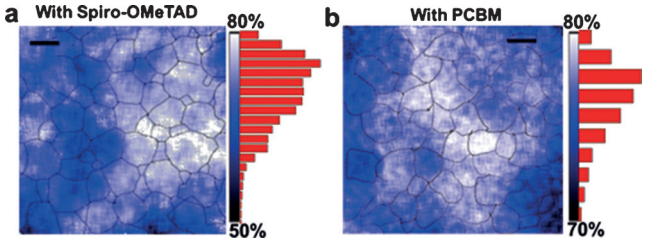

Figure 4. PL quenching efficiency (η) images of $CH_3NH_3PbI_3$ films after the depositions of a) Spiro-OMeTAD (hole acceptor) and b) PCBM (electron acceptor). Solid lines indicate grain boundaries. Scale bars: 5 μm. Besides the images are the histograms of quenching efficiency.

Our results show that polycrystalline perovskite films exhibit remarkably long and uniform carrier lifetimes, high and homogeneous intra-grain carrier diffusivities, and high average carrier extraction efficiencies at perovskite grain/electron (or hole) acceptor interface. This observation is consistent with high solar cell performance. However, there exists large (by up to 30%) grain to grain variation of carrier collection efficiencies. We attribute this to the presence of carrier extraction defects at some grain–electron (or hole) acceptor interface. Our results suggest that improving the homogeneity of grain–electron (or hole) acceptor contact is an important direction for further improvement of device performance. Furthermore, even in a high performing solar cell with thickness smaller than the carrier diffusion length, enhancing lateral inter-grain carrier diffusion would also be an important avenue for building in alternative carrier collection pathways to overcome defects at the grain/electrode interfaces.

Acknowledgements

S.J. acknowledges financial support from MOST (Grant No. 2016YFA0200602), National 1000 Young Talents Program of China, and Nature Science Foundation of Liaoning Province (Grant 2015021013). T.L. acknowledges the financial support from the US National Science Foundation (CHE-1309817).

Keywords: charge carriers · grain boundaries · perovskites · photoluminescence mapping · solar cells

How to cite: *Angew. Chem. Int. Ed.* **2016**, *55*, 13067–13071
Angew. Chem. **2016**, *128*, 13261–13265

[1] Research Cell Efficiency Records http://www.nrel.gov/ncpv (National Renewable Energy Laboratory, accessed 1 April 2016).
[2] S. D. Stranks, P. K. Nayak, W. Zhang, T. Stergiopoulos, H. J. Snaith, *Angew. Chem. Int. Ed.* **2015**, *54*, 3240–3248; *Angew. Chem.* **2015**, *127*, 3288–3297.
[3] A. Molina-Ontoria, I. Zimmermann, I. Garcia-Benito, P. Gratia, C. Roldan-Carmona, S. Aghazada, M. Graetzel, M. K. Nazeeruddin, N. Martin, *Angew. Chem. Int. Ed.* **2016**, *55*, 6270–6274; *Angew. Chem.* **2016**, *128*, 6378–6382.
[4] A. Kojima, K. Teshima, Y. Shirai, T. Miyasaka, *J. Am. Chem. Soc.* **2009**, *131*, 6050–6051.
[5] N. J. Jeon, J. H. Noh, W. S. Yang, Y. C. Kim, S. Ryu, J. Seo, S. I. Seok, *Nature* **2015**, *517*, 476–480.
[6] A. Y. Mei et al., *Science* **2014**, *345*, 295–298.
[7] J. Burschka, N. Pellet, S. J. Moon, R. Humphry-Baker, P. Gao, M. K. Nazeeruddin, M. Gratzel, *Nature* **2013**, *499*, 316–320.

© 2016 Wiley-VCH Verlag GmbH & Co. KGaA, Weinheim

[8] H. P. Zhou, Q. Chen, G. Li, S. Luo, T. B. Song, H. S. Duan, Z. R. Hong, J. B. You, Y. S. Liu, Y. Yang, *Science* **2014**, *345*, 542 – 546.
[9] L. M. Pazos-Outon et al., *Science* **2016**, *351*, 1430 – 1433.
[10] D. P. McMeekin et al., *Science* **2016**, *351*, 151 – 155.
[11] S. D. Stranks, G. E. Eperon, G. Grancini, C. Menelaou, M. J. P. Alcocer, T. Leijtens, L. M. Herz, A. Petrozza, H. J. Snaith, *Science* **2013**, *342*, 341 – 344.
[12] S. Kazim, M. K. Nazeeruddin, M. Gratzel, S. Ahmad, *Angew. Chem. Int. Ed.* **2014**, *53*, 2812 – 2824; *Angew. Chem.* **2014**, *126*, 2854 – 2867.
[13] H. Oga, A. Saeki, Y. Ogomi, S. Hayase, S. Seki, *J. Am. Chem. Soc.* **2014**, *136*, 16948 – 16948.
[14] C. Wehrenfennig, G. E. Eperon, M. B. Johnston, H. J. Snaith, L. M. Herz, *Adv. Mater.* **2014**, *26*, 1584 – 1589.
[15] R. Sheng, A. Ho-Baillie, S. J. Huang, S. Chen, X. M. Wen, X. J. Hao, M. A. Green, *J. Phys. Chem. C* **2015**, *119*, 3545 – 3549.
[16] C. S. Ponseca, et. al, *J. Am. Chem. Soc.* **2014**, *136*, 5189 – 5192.
[17] Q. Dong, Y. Fang, Y. Shao, P. Mulligan, J. Qiu, L. Cao, J. Huang, *Science* **2015**, *347*, 967 – 970.
[18] D. Shi et al., *Science* **2015**, *347*, 519 – 522.
[19] Z. G. Xiao, Q. F. Dong, C. Bi, Y. C. Shao, Y. B. Yuan, J. S. Huang, *Adv. Mater.* **2014**, *26*, 6503 – 6509.
[20] J. H. Heo et al., *Nat. Photonics* **2013**, *7*, 487 – 492.
[21] Y. H. Shao, Z. G. Xiao, C. Bi, Y. B. Yuan, J. S. Huang, *Nat. Commun.* **2014**, *5*, 5784.
[22] Z. G. Xiao, C. Bi, Y. C. Shao, Q. F. Dong, Q. Wang, Y. B. Yuan, C. G. Wang, Y. L. Gao, J. S. Huang, *Energy Environ. Sci.* **2014**, *7*, 2619 – 2623.
[23] W. Tian, C. Zhao, J. Leng, R. Cui, S. Jin, *J. Am. Chem. Soc.* **2015**, *137*, 12458 – 12461.
[24] J. S. Huang, Y. C. Shao, Q. F. Dong, *J. Phys. Chem. Lett.* **2015**, *6*, 3218 – 3227.
[25] D. W. de Quilettes, S. M. Vorpahl, S. D. Stranks, H. Nagaoka, G. E. Eperon, M. E. Ziffer, H. J. Snaith, D. S. Ginger, *Science* **2015**, *348*, 683 – 686.
[26] M. Vrućinić et al., *Adv. Sci.* **2015**, *2*, 1500136.
[27] C. G. Bischak, E. M. Sanehira, J. T. Precht, J. M. Luther, N. S. Ginsberg, *Nano Lett.* **2015**, *15*, 4799 – 4807.
[28] S. Draguta, S. Thakur, Y. V. Morozov, Y. Wang, J. S. Manser, P. V. Kamat, M. Kuno, *J. Phys. Chem. Lett.* **2016**, *7*, 715 – 721.
[29] M. J. Simpson, B. Doughty, B. Yang, K. Xiao, Y. Z. Ma, *J. Phys. Chem. Lett.* **2016**, *7*, 1725 – 1731.
[30] W. J. Yin, T. T. Shi, Y. F. Yan, *Adv. Mater.* **2014**, *26*, 4653 – 4658.
[31] J. S. Yun, A. Ho-Baillie, S. J. Huang, S. H. Woo, Y. Heo, J. Seidel, F. Z. Huang, Y. B. Cheng, M. A. Green, *J. Phys. Chem. Lett.* **2015**, *6*, 875 – 880.
[32] Y. Yamada, T. Yamada, L. Q. Phuong, N. Maruyama, H. Nishimura, A. Wakamiya, Y. Murata, Y. Kanemitsu, *J. Am. Chem. Soc.* **2015**, *137*, 10456 – 10459.
[33] A. Sharenko, M. F. Toney, *J. Am. Chem. Soc.* **2016**, *138*, 463 – 470.
[34] Z. Guo, J. S. Manser, Y. Wan, P. V. Kamat, L. B. Huang, *Nat. Commun.* **2015**, *6*, 7471.

Received: July 7, 2016
Published online: September 16, 2016

 © 2016 Wiley-VCH Verlag GmbH & Co. KGaA, Weinheim